NEW FRONT. CHEM. (2020) *Former: Ann. West Univ. Timisoara – Series Chem.*
Volume 29, Number 1, pp. 33-51 *ISSN: 1224-9513*
ISSN 2668-9189; ISSN-L 2393-2171

Article

MATRICEAL HETEROJUNCTIONS ON GRAPHENE. FIRST METROLOGICAL MEASUREMENTS

Doru BUZATU[1], Paula SVERA (Ianasi)[1,2], Mihai V. PUTZ [1,2,♣]

[1] National Institute for Research and Development in Electrochemistry and Condensed Matter, Laboratory of Renewable Energies – Scientific, Str. Prof. Paunescu-Podeanu 144, Timisoara 300569, Romania

[2] West University of Timisoara, Faculty of Chemistry-Biology-Geography, Biology – Chemistry Department, Laboratory of Structural and Computational Physical-Chemistry for Nanosciences and QSAR, Str. Pestalozzi 16A, Timisoara 300115, Romania

ABSTRACT

Tunable electrical properties of the graphene based materials have huge impact on the current technology expansion, leading to a possibility of multiple improvements of currently used materials, with the potential to develop novel applications. In this study electrical properties of GO/ZnO matrix deposited on ITO glass were investigated.

Keywords: graphene, matriceal heterojunctions

1. INTRODUCTION

Since its discovery, graphene along with the previously existent carbon allotropes have become part of multiple technologies and composite materials [1]. The properties of graphene include mechanical strength, superior thermal conductivity, transparency, high specific surface area, and excellent charge transport [2,3]. Good conductivity of the graphene can be attributed to the position of p orbitals which result in delocalized π bonds moving freely in the whole graphene plane [4]. As a consequence, high conductivity of graphene could be explained by the presence of zero-energy band gap. More precisely, the place where π∗-state conduction band (CB) and the π-state valence band (VB) touch each other result in Dirac point [5].

Starting from the electronic structure of the graphene, sp2 hybridization between one s orbital and two p orbitals results in a trigonal planar structure, creating σ bond between carbon

♣ Correspondent author: mihai.putz@e-uvt.ro

atoms which is adhered to the lattice structure firmness. From this point, unaffected p orbital forms covalent bond with neighboring carbon atoms, resulting in the appearance of π band. Because each p orbital has one extra electron, the π band will be half filled [6].

Introduction of the foreign atoms and defect sites on the lattice of graphene, which highly influence its electrical properties [6,7], is the main cause for the ambivalent nature of the graphene, resulting in a p-type or an n-type semiconductor [8].

A tunable band gap however, could be obtained from insulating to conducting by controlling the reduction degree of rGO, as the band gap energy is strongly correlated with the number of oxidized sites, and the oxidization degree of rGO [9].

The importance of half-filled bands is reflected in large Coulomb energies that cause strong collective effects, magnetism, and insulating behavior of the materials [10]. Taking into account the resonant valence bond structure of the graphene and its semimetal-like behavior, the result is unusual linearly dispersing electronic excitations called Dirac electrons. The importance of the band structure along with the Dirac points is reflected in the graphene properties like high conductivity and electron mobility (Figure 1a and Figure 2) [6,11].

The carrier concentration can be tuned from holes to electrons, which depends of the applied gate voltage, as result having bipolar field effect. Considering the thermal fluctuations, non-uniformities in the material, impurities, electrical charges in the vicinity of graphene, some residual charge carrier concentration may exist in graphene devices [11].

In this work the aim was to study the graphene-oxide/TiO2 semiconductors with tunable conductivity, placed in a specific matriceal sequence, in order to predict a conductivity pattern based on quantic effects that take place. It is presumed that the non-contact depositions placed at micrometric distances will induce new interactions (Figure 1b).

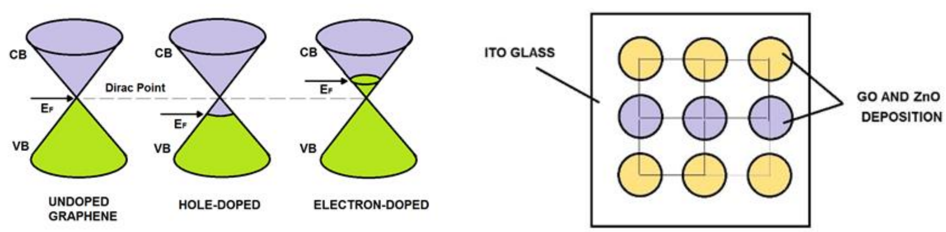

Figure 1. *a): Dirac point position in case of undoped graphene, hole-doped graphene and electron-doped graphene; b): Matriceal depositions of GO/TiO2 on ITO glass*

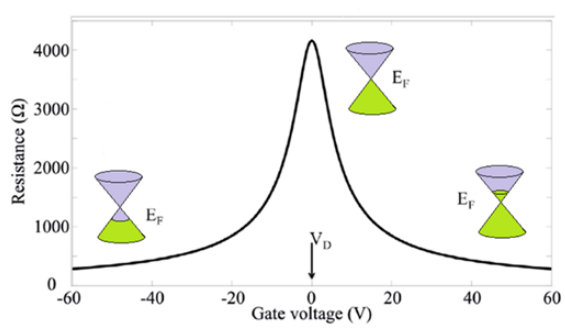

Figure 2*. Resistance vs Gate voltage dependence for graphene, showing the Dirac point (VD), where resistance reaches a maximum. In this case the Dirac point is at VD = 0 (neutrality point). By applying positive gate voltages, n-doped (electron doped) graphene is made, and vice-versa for p-doped graphene where negative voltages are applied. EF marks the Fermi energy [6,11]*

2. METHOD/MODEL

Quantum mechanics represents an efficient approach for defining accurate and substantial scientific theory [12-15]. Relevant phenomena that occurs in quantum mechanics is superposition and entanglement, that also enables quantum computers to perform, using a variety of physical technologies, such as trapped ions, superconductors or photons. What is common for each approach is the quantum noise, for this reason quantum mechanics states require isolation from the environment. In order to achieve fully functional quantum computers, design of correct algorithms together with error correcting codes is of great importance. In quantum mechanics there are phenomena that are inexistent in classical physics for example the occurrence of two distinct states of the same system [16], whereas the transition between these two states is represented by logical operations. The multiple quantum states are described as qubits when two states are present and qudits when the system number is higher. Because quantum systems can exist simultaneously, a qubit can be either 1 and 0, a property attributed to the superposition. Other advantage is entanglement, a phenomenon which is referred to the dependence between the qubits. Combined together, superposition and entanglement, create main power of quantum computing, named quantum parallelism.

Because qubit's two states are represented in binary information and exist in the same time due to the superposition, the contained information can be described as [12,15]:

$$\alpha |0\rangle + \beta |1\rangle$$

where α and β, are the complex numbers called amplitudes. $|0\rangle$ and $|1\rangle$ are the possible states of the qubit, referred as kets. Using this formula, it can be obtained the quantity of the 0 and 1 provenience of the qubit state. Determination of the qubit state probability is possible with the following formula:

$$\mathrm{prob}(0) = |\alpha |2$$

$$\mathrm{prob}(1) = |\beta |2$$

$$|\alpha |2 + |\beta |2 = 1$$

Because qubit must be defined in one of the two states, it could be more complicated when α and β contain negative values or imaginary parts. From this point such attributes allow the occurrence of phase difference between the states $|0\rangle$ and $|1\rangle$. In addition, this notation can be expanded to multiple independent qubits combined, for example:

$$\alpha |0\rangle + \beta |1\rangle \text{ and } \gamma |0\rangle + \delta |1\rangle$$

represented by a tensor product:

$$(\alpha |0\rangle + \beta |1\rangle) \otimes (\gamma |0\rangle + \delta |1\rangle)$$

For entangled states, the following state is suitable:

$\alpha\gamma\, |00\rangle + \alpha\delta\, |01\rangle + \beta\gamma\, |10\rangle + \beta\delta\, |11\rangle$

In the case of entangled states, it is not possible to represent independent qubits, more precisely the quantum state cannot be described by each qubit's specific state, therefore an example of entangled state can be presented as:

$\alpha\, |00\rangle + \beta\, |11\rangle$

Using Bell's quantum teleportation principle, both qubit states are distinguished by measuring only one of the qubit states. Starting with the previous statement, coefficients for $|01\rangle$ and $|10\rangle$ are 0 in case of two qubits, as for final determination, the system must be either in $|00\rangle$ or $|11\rangle$ state.

Other important factor in determining the quantum states is the amplitude. The role of the amplitude is to operate as variable of the quantum algorithm, more precisely, in an n qubit system exist 2n amplitudes. The only disadvantage is that the amplitude cannot be measured directly, whereas when qubits are measured, amplitude is compelled to be either 0 or 1 [12,15].

Because quantum operations overwrite the data in the process, this inconvenience is solved by using approximate computing. Quantum computing is probabilistic by nature; therefore, quantum states are hard to define. Taking into account the existent quantum algorithms (Shor, QFT, Grover, Simon, Deutsch-Josza) approximation algorithms proved to be more suitable highlighting the fact that they can run on near-term, error prone quantum computers [12,17]. In the process, entangled states are directed towards a target state that can minimize a cost function using variation of quantum gate parameters [12, 18].

Other complementary approaches to the quantum algorithms that should be taken into consideration are the error correction and potential for scaling.

In case of quantum computers, the error correction is very important because of the present noise which is also the main reason for the yet inexistent large-scale computers, mainly because the interaction with the environment (or external medium) will damage the quantum state. Because of the fragility that exhibit the existent error correction codes, extra qubits are observed, which have the main goal to interact with the qubits that hold the state.

On the other hand, physical performance of quantum computation implementation is possible using molecular magnets [19], NMR spectroscopy [20], photons [21], non-Abelian anions [22], trapped ions [23], Quantum Dots [24], and superconductors [12]. Undeniably, for each approach there is a specific system that can describe the process, still there are several conditions that apply to all:

- Quantum information that must exist even in most rudimental state
- Ability to perform a universal family or unitary transformations
- Execution/preparation of a credible and trusted initial state
- Measurement of the resulted output

The first criteria is referred to the necessity for a reliable usage and storage of the information, a property that is extensively used in classical computers. The second item is referred to the universal set that also allows linear transformations. The last two criteria are related to the classical creation and measurement of states. More precisely, quantum computer should perform arbitrary quantum operations and to have the ability be controlled and measured in a “classical” manner. Still other factors need to be considered, more exactly when evaluating the conditions starting from a physics device, values like coherence time, gate latency, gate fidelity and mobility are crucial, while from an engineering viewpoint, topology (qubit connectivity), maturity, ease of fabrication, control and integration have relevance [12,15].

What is significant in this study is the fact that superconductors rely on the sequence of swap gates in order to move quantum states. Following this direction coupling over long distance superconducting transmission lines could be a new alternative for the superconductors. A milestone in this regard is the fact that superconducting computers have immobile qubits resulting in a better topology involving a better determination of which qubit can interact. At the same time this will have as consequence long distance communication and also swap gates, with a resulting increasing number of required gates. Number of the qubits can determine an increase of gates in the actual system. In comparison to the other existent technologies’ semiconductor and superconductor-based applications are the most appropriate for quantum computers. One example is superconducting computers based on Josephson junctions built with traditional circuit design and produced physically with the aid of lithography [25].

Still after all the benefits of superconductors and semiconductors in quantum computer applications, the existence of reliable physical quantum gates still persists. Quantum technologies use analog signals for operations yet quantum operations are time sensitive, that in consequence can result in delay of pulse on the order of couple nanoseconds which is reflected in an incorrect operation. In addition, superconducting computers require higher number of currents carrying wires which can affect the reliability of the output [12]. This problem was solved by operating at very low temperatures (around 0K) [26]. Due to very demanding conditions of operating at low temperatures and because circuits typically operate at warmer temperature than the qubits, temperature of 4K is more suitable for testing.

3. RESULTS

2.1. ZnO and GO matrix deposition on ITO glass

Deposition of GO and ZnO was carried out by drop casting on glass and ITO glass substrate, following a determined matrix pattern as showed in the Figure 3. For the following depositions, one type of ZnO paste and 3 variations of GO were obtained, following two sources of graphene oxide in water dispersia, that were reduced as indicated in preparation of X1, X2 and Y2.

2.1.1. Preparation of ZnO paste

0.4 g of ZnO (purchased from Sigma-Aldrich) was weighted and milled, followed by an addition of 12 drops of water. After mixing the ZnO and water, 0.08 ml of glacial acetic acid was added. After mixing the compounds, 8 drops of triton x 45 were added.

2.1.2. Preparation of rGO (X1)

GO (graphene oxide in water dispersion previously obtained by Cataldo et al. [27]) was mixed with 1 mL of 1-ascorbic acid (1M) and left for one hour in the ultrasonic bath at 60 ° C. The mixture was then exposed to a temperature of 90 ° C. 0.45 mL of hydrogen peroxide was then added and the mixture was left for 30 minutes at 60 ° C in the ultrasonic bath.

2.1.3. Preparation of rGO (X2)

GO (graphene oxide in water dispersion previously obtained by Cataldo et al. [27]) was mixed with 1 mg of L- ascorbic acid and left for one hour in the ultrasonic bath at 60 ° C.

2.1.4. Preparation of rGO (Y2)

GO (commercial graphene oxide in water dispersa purchased from Sigma-Aldrich) was mixed with 1 mg of L- ascorbic acid and left for one hour in the ultrasonic bath at 60 ° C.

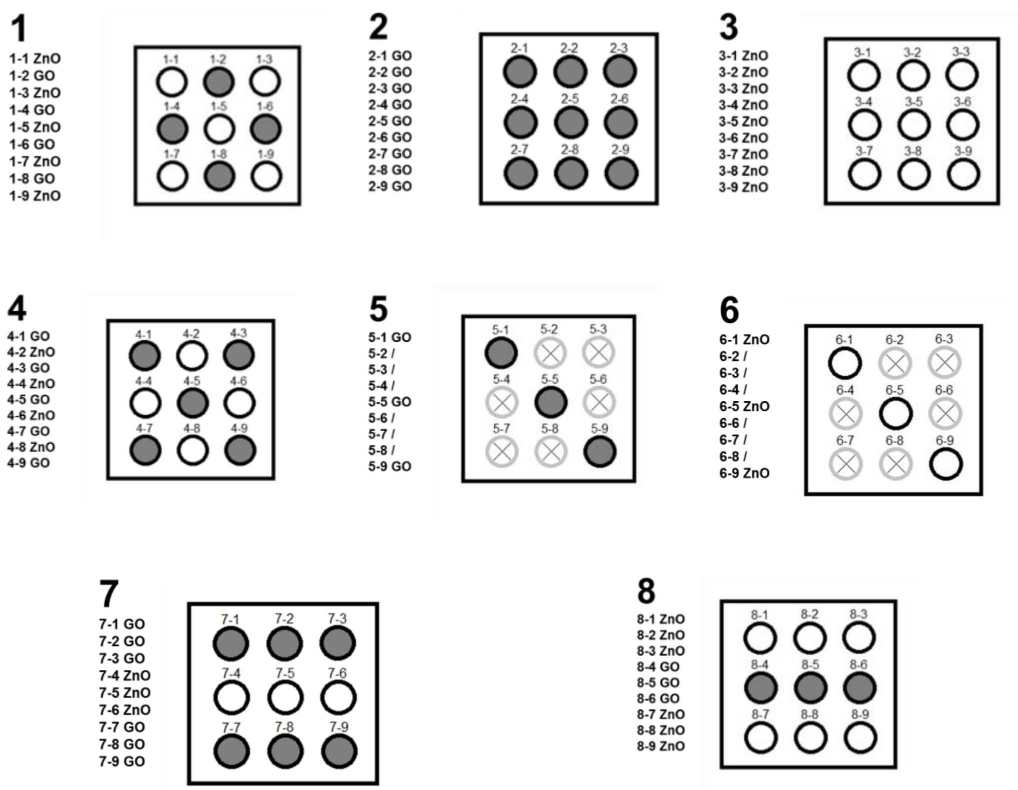

Figure 3. *Matrix pattern of ZnO and GO deposited on ITO glass: Plate 1; Plate 2; Plate 3; Plate 4; Plate 5; Plate 6; Plate 7; and Plate 8.*

2.2. Electrical resistance, electrical voltage and electric current intensity of the deposited materials (GO/ZnO matrix)

The first electrical resistance measurement was performed on ITO plate. It has been observed that measurements at different distances result in different resistance values. Thereby, measurements were performed at the same distance for all the deposited plates, indicating 20 Ω for undeposited ITO plate.

Before the electric measurements of the sample, rezistance of each deposition line was checked, indicating hight variations in case of X1 (up to 1770 Ω), and small variations in case of X2 and Y2 (Figure 4).

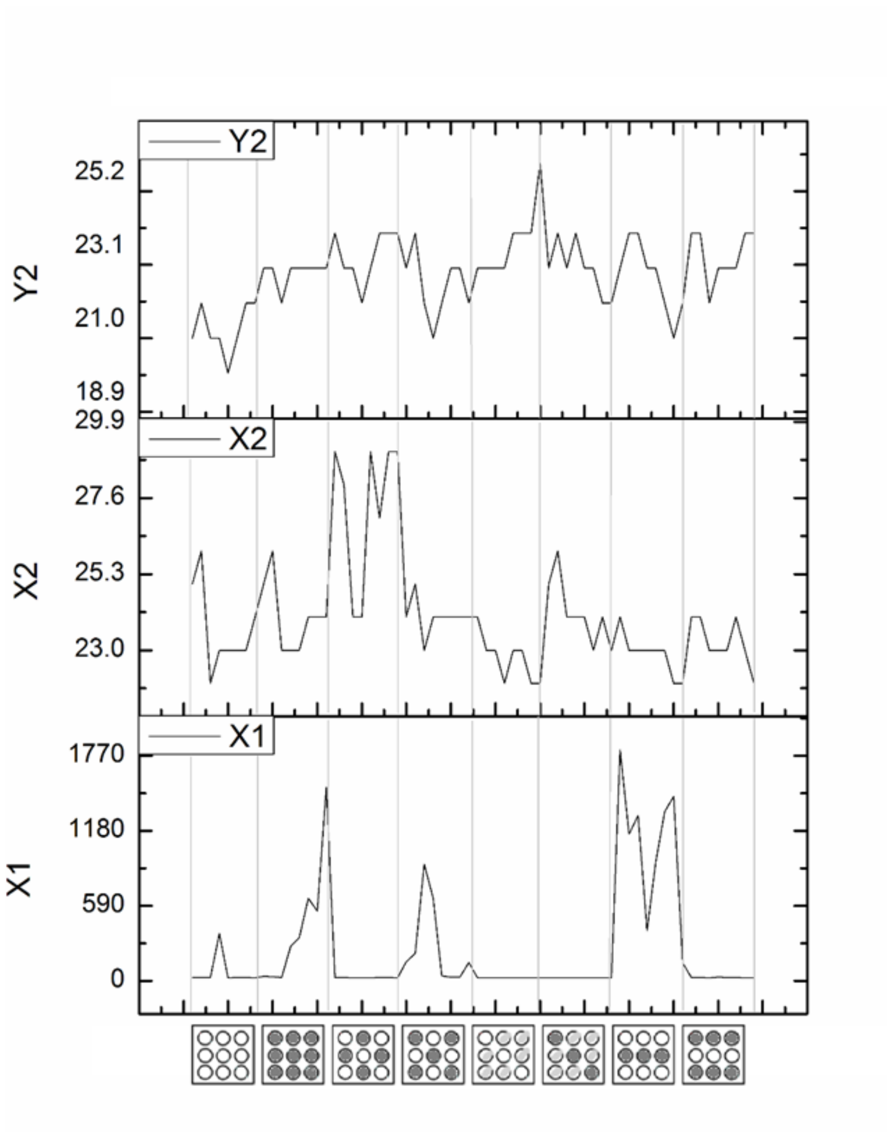

Figure 4. *Rezistance measurements: range and variations of samples X1, X2 and Y2.*

Electric measurements were performed with the aid of a multimeter which was connected to a resistance and a baterry (Figure 5). In the first phase, U, I and R values were registered in the absence of the deposited plate. With the deposited sample in circuit, no differences in R and U were observed. All in all, the results are presented in Table 1.

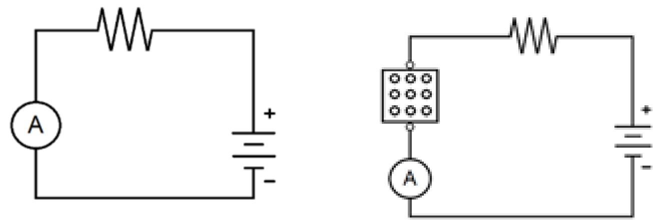

Figure 5. *Circuit scheme: without (left) and with (right) the deposited sample.*

Table 1. *Electric measurements for sample X1, X2 and Y2 at different temperatures (25, 40 and 10°C) and in the presence of a magnet*

		Current intensity [mA] at 25˚C			**Current intensity [mA] at 40˚C**			**Current intensity [mA] at 10˚C**			**Current intensity [mA] at 25˚C and in presence of magnet**		
Plate 1													
Measuring area	Deposition number	X1	X2	Y2	X1 40	X2 40	Y2 40	X1 10	X2 10	Y2 10	X1 m	X2 m	Y2 m
Values of U, I and R during the entire measurement		1.35 V, 10.18 mA, 1811 Ω	1.33 V, 10.09 mA, 1727 Ω	1.35 V, 10.14 mA, 1800 Ω	1.35 V, 10.28 mA, 1788 Ω at 40˚ C	1.34 V, 10.16 mA, 1759 Ω at 40˚ C	1.32 V, 10.21 mA, 1700 Ω at 40˚ C	1.31 V, 10.11 mA, 1684 Ω at 10˚ C	1.32 V, 10.16 mA, 1690 Ω at 10˚ C	1.33 V, 10.14 mA, 1751 Ω at 10˚ C	1.33 V, 10.07 mA, 1737 Ω	1.33 V, 10.09 mA, 1727 Ω	1.33 V, 10.05 mA, 1727 Ω
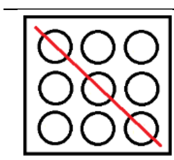	3-1 – 3-9	8.6	0.8-6	8.6	8.6	0-7	8.6	4-6.7	6-8.3	8.5	7-8.3	1.7-7.8	8.3
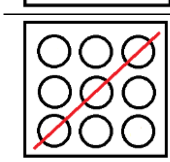	3-3 – 3-7	8.5	3-8	8.6	8.5	8.5	8.6	0-6.5	6-8.2	8.6	6-8.4	5-8.2	7-8.3

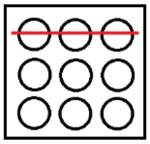	3-1 – 3-3	8.6	5-8	8.6	8.7	6.8-8.3	8.6	0-5	6-8.4	8.6	6-8.2	5.5-8.1	8.4
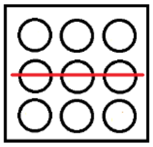	3-4 – 3-6	4-8.6	7-8.4	8.6	8.7	0-8	8.6	1-6.4	7.8-8.5	8.7	6-8.4	6.8-8.3	8.5
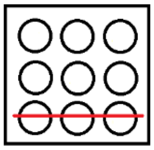	3-7 – 3-9	8.2	0.8-7	8.6	0-8.1	0-6.3	8.7	2-6.7	6-8.3	8.7	6-8.4	5.8-7.3	8.5
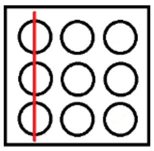	3-1 – 3-7	8.6	8.2-8.4	8.6	8.6	0-8.4	8.6	7-8.4	8-8.4	8.5	7-8.3	7.6-8.4	6-8.4
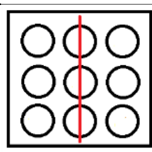	3-2 – 3-8	8.6	8-8.4	8.6	8.6	6-8.3	8.7	7-8.4	8.2-8.5	8.5	7-8.3	3.2-7.9	8.5
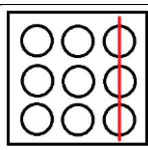	3-3 – 3-9	8.6	7.4-8.4	8.7	8.6	6-7.6	8.7	4-8.2	7.8-8.5	8.6	6-8.4	0.1-7.2	8.5

Plate 2

Measuring area	Deposition number	X1	X2	Y2	X1 40	X2 40	Y2 40	X1 10	X2 10	Y2 10	X1 m	X2 m	Y2 m
Values of U, I and R during the entire measurement		1.36 V, 10.18 mA, 1818 Ω	1.33 V, 10.11 mA, 1742 Ω	1.35 V, 10.15 mA, 1804 Ω	1.34 V, 10.33 mA, 1782 Ω at 40° C	1.34 V, 10.17 mA, 1759 Ω at 40° C	1.33 V, 10.21 mA, 1709 Ω at 40° C	1.32 V, 10.03 mA, 1691 Ω at 10° C	1.32 V, 10.16 mA, 1693 Ω at 10° C	1.34 V, 10.13 mA, 1755 Ω at 10° C	1.35 V, 10.05 mA, 1739 Ω	1.33 V, 10.11 mA, 1742 Ω	1.33 V, 10.05 mA, 1739 Ω
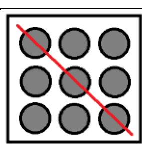	2-1 – 2-9	1.36	8.5	8.6	7-8.2	8.4	8.6	3-7.9	8.2-8.5	8.5	8.5	8.4	8.5

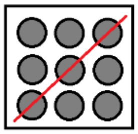	2-3 – 2-7	0.2-7.4	8.5	8.6	1-7.7	8.5	8.7	5-7.5	6-8.2	8.6	8.5	7-8.3	8.5
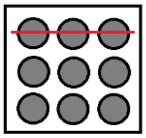	2-1 – 2-3	2-5.3	8.6	8.7	2-7.3	8.5	8.8	0-3	8.5-8.6	8.6	8.6	6-8.4	8.6
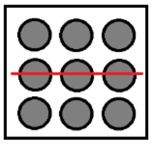	2-4 – 2-6	0.2-5.2	6.9-8.4	8.7	1.9-5.9	8.5	8.7	7-8.3	7-8.4	8.6	8.6	7.9-8.4	8.6
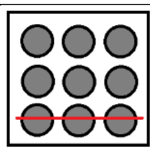	2-7 – 2-9	2-8	8.6	8.6	1.2-4	8.6	8.7	6-8.2	7-8.5	8.6	8.5	8.4	8.5
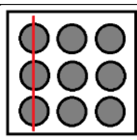	2-1 – 2-7	6-8.3	8.6	8.7	8.4-8.5	8.6	8.7	4-7.1	8.4-8.5	8.6	8.5	8.4-8.5	8.5
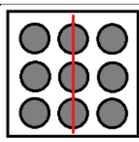	2-2 – 2-8	3-6	8.5	8.8	4-7.2	8.5	8.7	5-7.8	0-8.3	8.6	8.6	8.5	8.6
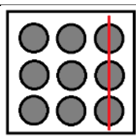	2-3 – 2-9	0.1-2	8.6	8.6	5-7.3	8.5	8.7	0-7	7-8.6	8.6	8.6	8.6	8.6
Plate 3													
Measuring area	Deposition number	X1	X2	Y2	X1 40	X2 40	Y2 40	X1 10	X2 10	Y2 10	X1 m	X2 m	Y2 m
Values of U, I and R during the entire measurement		1.36 V, 10.12 mA, 1846 Ω	1.33 V, 10.12 mA, 1747 Ω	1.35 V, 10.12 mA, 1814 Ω	1.34 V, 10.22 mA, 1786 Ω at 40° C	1.34 V, 10.14 mA, 1776 Ω at 40° C	1.33 V, 10.21 mA, 1714 Ω at 40° C	1.32 V, 10.07 mA, 1694 Ω at 10° C	1.32 V, 10.18 mA, 1694 Ω at 10° C	1.34 V, 10.09 mA, 1762 Ω at 10° C	1.33 V, 10.05 mA, 1730 Ω	1.34 V, 10.10 mA, 1754 Ω	1.34 V, 10.14 mA, 1779 Ω
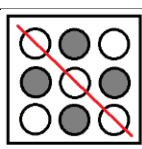	1-1 – 1-9	8.5	8.6	8.6	8.6	8.7	8.7	0-7	8.6	8.7	3-7.4	8.6	8.7

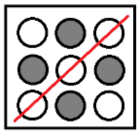	1-3 – 1-7	7-8.4	8.6	8.6	8.6	8.6	8.7	3-8	8.6	8.6	6-8.2	8.6	8.6
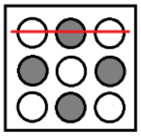	1-1 – 1-3	1.9-8.2	8.6	8.7	4-8.2	8.7	8.8	0-7	8.6	8.6	6-8.4	8.6	8.7
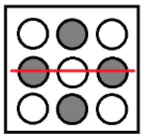	1-4 – 1-6	0.4-8.5	8.6	8.7	8.6	8.6	8.8	4-8.2	8.6	8.7	0-7.4	8.6	8.7
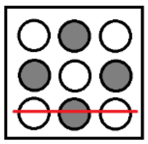	1-7 – 1-9	1.6-8.1	8.6	8.6	8.6	8.7	8.8	0-7.5	8.6	8.6	5-8.4	8.6	8.8
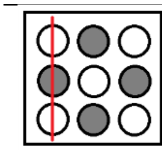	1-1 – 1-7	8.3	8.7	8.7	8.6	8.7	8.7	3.3-8.2	8.6	8.6	3-7.8	8.6	8.7
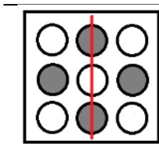	1-2 – 1-8	4-8	8.7	8.8	8.6	8.7	8.8	7-8.4	8.6	8.6	6-8	8.6	8.7
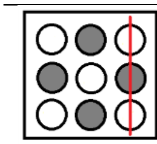	1-3 – 1-9	8.6	8.6	8.6	8.6	8.7	8.8	6.9-8.2	8.7	8.6	0-4	8.6	8.7
Plate 4													
Measuring area	Deposition number	X1	X2	Y2	X1 40	X2 40	Y2 40	X1 10	X2 10	Y2 10	X1 m	X2 m	Y2 m
Values of U, I and R during the entire measurement		1.35 V, 10.20 mA, 1808 Ω	1.33 V, 10.04 mA, 1718 Ω	1.35 V, 10.16 mA, 1795 Ω	1.34 V, 10.22 mA, 1776 Ω at 40° C	1.34 V, 10.20 mA, 1746 Ω at 40° C	1.32 V, 10.18 mA, 1699 Ω at 40° C	1.31 V, 10.18 mA, 1681 Ω at 10° C	1.32 V, 10.17 mA, 1680 Ω at 10° C	1.33 V, 10.12 mA, 1745 Ω at 10° C	1.33 V, 10.05 mA, 1728 Ω	1.33 V, 10.04 mA, 1718 Ω	1.33 V, 10.06 mA, 1720 Ω
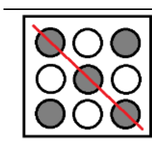	4-1 – 4-9	0-1	8.5	8.6	5-7.4	5-7.8	8.7	7-8.6	6.2-8.2	8.6	2-6.2	6.2-8.1	8.5

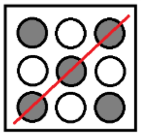	4-3 – 4-7	4-8	7.8-8.3	8.6	9.3	7-8.5	8.6	8.4	6.8-8.2	8.6	7-8.4	7.8-8.3	8.6
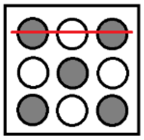	4-1 – 4-3	1.4-5.3	8.2-8.4	8.7	5.2-7	4.3-8.4	8.7	8.6	5.6-7.6	8.7	0-3	3.6-7.4	8.5
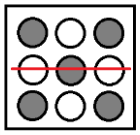	4-4 – 4-6	0.6-7	8.2-8.3	8.7	4.3-5.6	6-8.2	8.7	8.6	4-7.7	8.6	0-6	2.7-8	8.6
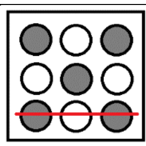	4-7 – 4-9	3-7	8.6	8.7	3-7.7	8.6	8.6	8.4	6-8.2	8.6	0-7.6	7.2-8.4	8.5
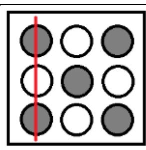	4-1 – 4-7	4-8.4	8.4	8.7	4.5-8	8-8.4	8.7	8.6	8-8.5	8.7	0-8.5	5.2-8.4	8.7
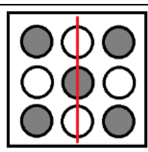	4-2 – 4-8	0.5-5	8.5	8.6	5-8.3	5-8.5	8.7	8.6	5.3-8.3	8.6	7-8.2	5.1-8.3	8.6
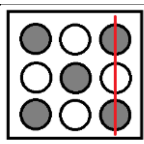	4-3 – 4-9	1-5	7.3-8.5	8.7	5-8.4	8.3	8.7	8.5	6.8-8.6	8.6	6-8.2	4.8-7.4	8.6

Plate 5

Measuring area	Deposition number	X1	X2	Y2	X1 40	X2 40	Y2 40	X1 10	X2 10	Y2 10	X1 m	X2 m	Y2 m
Values of U, I and R during the entire measurement		1.35 V, 10.20 mA, 1791 Ω	1.32 V, 10.15 mA, 1699 Ω	1.34 V, 10.14 mA, 1788 Ω	1.34 V, 10.30 mA, 1770 Ω at 40° C	1.33 V, 10.19 mA, 1730 Ω at 40° C	1.32 V, 10.18 mA, 1693 Ω at 40° C	1.31 V, 10.19 mA, 1672 Ω at 10° C	1.31 V, 10.17 mA, 1680 Ω at 10° C	1.33 V, 10.08 mA, 1732 Ω at 10° C	1.32 V, 10.06 mA, 1715 Ω	1.32 V, 10.15 mA, 1699 Ω	1.33 V, 10.17 mA, 1707 Ω
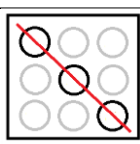	6-1 – 6-9	8.6	8.2-8.4	8.6	8.5	5-7.5	8.6	8.6	8.1-8.5	8.6	8.5	4-8.4	8.6

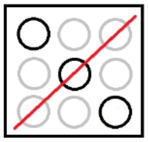	6-3 – 6-7	8.8	6.6-8.4	8.6	8.7	5-8.5	8.6	8.6	7.6-8.4	8.6	8.5	0-7.8	8.6
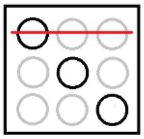	6-1 – 6-3	8.7	6.7-8.3	7-8.5	8.7	7-8.6	8.7	8.6	8.3-8.5	8.7	8.5	6.4-8.3	8.7
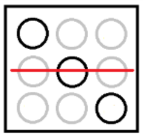	6-4 – 6-6	8.6	7-8.6	6.6-8.4	8.6	8-8.5	8.7	8.6	8-8.5	8.7	8.4	1-8.4	8.6
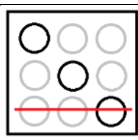	6-7 – 6-9	8.5	2.3-8	8.5	8.6	8.6	8.7	8.6	8.1-8.5	8.6	8.5	7.9-8.5	8.6
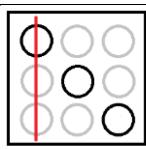	6-1 – 6-7	8.6	8.1-8.6	8.7	8.7	7.8-8.7	8.7	8.7	7-8.4	8.7	8.5	7.8-8.5	8.6
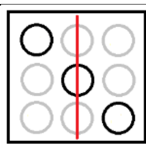	6-2 – 6-8	8.7	7.6-8.5	8.7	8.7	8.5	8.7	8.6	6.8-8.5	8.7	8.6	1-8.4	8.7
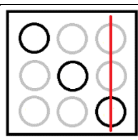	6-3 – 6-9	8.8	8.6	8.7	8.7	8.5	8.7	8.6	6.6-8.5	8.7	8.5	7-8.6	8.7

Plate 6

Measuring area	Deposition number	X1	X2	Y2	X1 40	X2 40	Y2 40	X1 10	X2 10	Y2 10	X1 m	X2 m	Y2 m
Values of U, I and R during the entire measurement		1.35 V, 10.19 mA, 1790 Ω	1.32 V, 10.07 mA, 1705 Ω	1.35 V, 10.16 mA, 1792 Ω	1.34 V, 10.21 mA, 1772 Ω at 40° C	1.33 V, 10.19 mA, 1733 Ω at 40° C	1.32 V, 10.19 mA, 1696 Ω at 40° C	1.31 V, 10.14 mA, 1675 Ω at 10° C	1.31 V, 10.17 mA, 1682 Ω at 10° C	1.33 V, 10.11 mA, 1740 Ω at 10° C	1.33 V, 10.04 mA, 1722 Ω	1.32 V, 10.16 mA, 1701 Ω	1.33 V, 10.05 mA, 1718 Ω
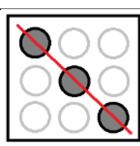	5-1 – 5-9	8.6	8.5	3-6	8.6	8.6	4.8-8.2	8.7	8.7	4-8.2	8.5	8.6	0-6

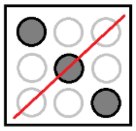	5-3 – 5-7	8.6	8.6	3-7.4	0-6	8.6	3.8-8.4	8.7	8.7	5-8	8.6	8.6	1-6.6
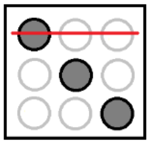	5-1 – 5-3	8.7	8.7	4-7.8	8.7	8.7	6-8.3	8.7	8.7	5-8.2	8.5	8.6	1-5
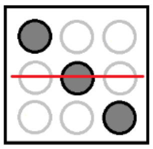	5-4 – 5-6	8.8	8.7	3-7.8	8.7	8.7	5-8.3	8.7	8.7	4-8.4	8.6	8.6	1-5.6
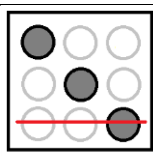	5-7 – 5-9	8.6	8.7	3.2-7.6	8.7	8.7	8.6	8.7	8.7	5-8.2	8.6	8.6	2-6.6
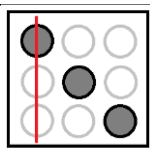	5-1 – 5-7	8.7	8.6	2.3-5	8.6	8.8	6.8-8.4	8.6	8.7	5-8.2	8.7	8.6	0-5
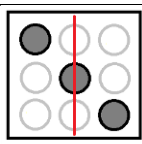	5-2 – 5-8	8.6	8.6	0-5	8.8	8.8	5-8.1	8.7	8.7	5-8.4	8.7	8.5	1-6.6
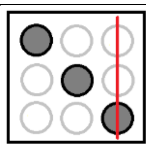	5-3 – 5-9	8.8	8.7	2-7.3	8.8	8.7	6-8.2	8.7	8.7	5-8.4	8.7	8.7	1-6

Plate 7

Measuring area	Deposition number	X1	X2	Y2	X1 40	X2 40	Y2 40	X1 10	X2 10	Y2 10	X1 m	X2 m	Y2 m
Values of U, I and R during the entire measurement		1.35 V, 10.2 mA, 1790 Ω	1.32 V, 10.15 mA, 1688 Ω	1.34 V, 10.15 mA, 1781 Ω	1.34 V, 10.18 mA, 1768 Ω at 40° C	1.33 V, 10.20 mA, 1717 Ω at 40° C	1.32 V, 10.18 mA, 1686 Ω at 40° C	1.31 V, 10.19 mA, 1661 Ω at 10° C	1.31 V, 10.18 mA, 1674 Ω at 10° C	1.33 V, 10.12 mA, 1726 Ω at 10° C	1.32 V, 10.03 mA, 1710 Ω	1.32 V, 10.15 mA, 1688 Ω	1.32 V, 10.20 mA, 1704 Ω

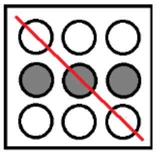	8-1 – 8-9	8.6	8.5	8.6	8.6	8.6	8.5	8.5	8.5	8.6	8.3	8.5	8.7
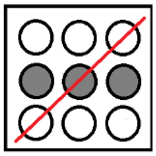	8-3 – 8-7	8.6	8.6	8.6	8.4	8.6	8.6	8.5	8.5	8.6	8.5	8.5	8.5
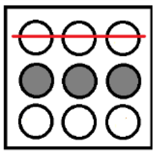	8-1 – 8-3	8.7	8.6	8.7	8.6	8.6	8.6	8.6	8.6	8.6	8.5	8.6	8.7
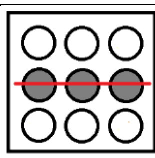	8-4 – 8-6	6-8.7	8.6	8.7	8.6	8.7	8.6	8.5	7-8.6	8.6	7-8.4	8.5	8.6
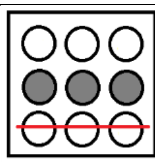	8-7 – 8-9	4-6.7	8.5	8.6	8.6	8.6	8.6	8.6	8.6	8.6	4-8.3	8.5	8.6
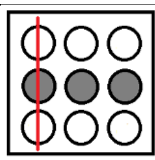	8-1 – 8-7	8.6	8.6	8.7	8.5	8.7	8.6	8.6	8.6	8.6	8.5	8.6	8.7
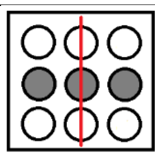	8-2 – 8-8	8.6	8.6	8.7	8.5	8.7	8.6	8.6	8.6	8.6	6-8.3	8.6	8.7
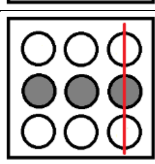	8-3 – 8-9	8.7	8.6	8.7	8.7	8.7	8.6	8.6	8.7	8.7	8.4	8.6	8.7

Plate 8

Measuring area	Deposition number	X1	X2	Y2	X1 40	X2 40	Y2 40	X1 10	X2 10	Y2 10	X1 m	X2 m	Y2 m
Values of U, I and R during the entire measurement		1.35 V, 10.20 mA, 1792 Ω	1.32 V, 10.17 mA, 1693 Ω	1.34 V, 10.16 mA, 1785 Ω	1.34 V, 10.31 mA, 1768 Ω at 40° C	1.34 V, 10.19 mA, 1746 Ω at 40° C	1.32 V, 10.18 mA, 1691 Ω at 40° C	1.31 V, 10.19 mA, 1669 Ω at 10° C	1.31 V, 10.16 mA, 1678 Ω at 10° C	1.33 V, 10.12 mA, 1729 Ω at 10° C	1.32 V, 10.03 mA, 1710 Ω	1.32 V, 10.17 mA, 1693 Ω	1.33 V, 10.15 mA, 1706 Ω

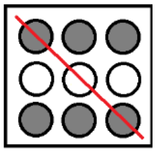	7-1 – 7-9	0.7-5	8.7	8.6	0.9-8	8.6	8.6	5-8.2	8.6	8.6	0-3.6	8.6	8.7
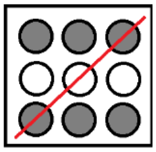	7-3 – 7-7	2-6	8.5	8.6	8.3	8.6	8.6	8.4	8.6	8.5	0-3.6	8.6	8.6
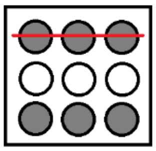	7-1 – 7-3	0.7-5	8.6	8.7	4-5.3	8.6	8.7	8.5	8.6	8.6	0-5.7	8.7	8.6
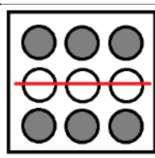	7-4 – 7-6	0-0.8	8.6	8.7	0.6-7.3	8.6	8.6	8.6	8.6	8.6	0-6.8	8.7	8.7
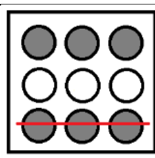	7-7 – 7-9	0.2-1.3	8.6	8.7	3-8.6	8.6	8.5	7-8.3	8.7	8.6	0-4.2	8.6	8.6
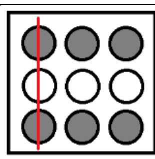	7-1 – 7-7	4-6	8.7	8.7	1.4-8	8.6	8.6	1-7	8.7	8.7	0-3.8	8.7	8.7
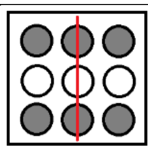	7-2 – 7-8	0-2	8.7	8.7	0.3-1.3	8.7	8.7	6-8.4	8.8	8.7	0-5.2	8.6	8.6
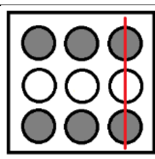	7-3 – 7-9	0-0.3	8.7	8.7	3-7	8.7	8.7	6-8.2	8.6	8.6	0-5.1	8.7	8.6

4. CONCLUSIONS

Besides its excellent properties, graphene has also a great potential for detecting the light. Much more important, its ability stands in identifying the light of any color, as a result of fast electronic response, a process described by Tomadin et al. [28]. It was observed that light absorption has an impact on graphene's conductivity, implying both increase and decrease of conductivity. One cause is that in the moment when graphene absorbs light, electrons heat extremely fast. In case of highly doped graphene, which as a result contains numerous free electrons, electron heating caused by the absorption of light leads to a decreased conduction. On the other hand, weakly doped graphene with less free electrons exhibits increased conductivity due to the formation of free electrons after the light absorption and therefore the created heat positively influences the conductivity of graphene materials.

Furthermore, a desirable feature of any quantum processor is rapid and accurate readout of the qubit states, for this reason most efficient readout technique uses readout resonators coupled to each qubit (circuit QED architecture), although few experimental studies were reported. Among the tested materials are van der Waals multilayered materials (vdW) that include insulators, semiconductors, superconductors and magnetic materials [29]. Wang et al. developed vdW voltage-tunnable heterostructures with graphene and semiconductor and observed the appearance of bipolar Josephson current in the ballistic regime. Despite the unusual Dirac band structure formed in graphene, the used qubit configuration facilitated access to electronic gate voltage tunning [30-33].

The present work discusses obtained results of graphene-oxide/ZnO depositions, in 3Qubit configuration, i.e. 8x8 matrix-junction; with the aim to implement various local metal-oxide quantum transistor configurations in future works. More precisely, under applied voltage, the input logical signals (AND, OR, XOR), together with the structural physical-chemical oxides combinations operate as the quantum gate-source-drain connections, so that the obtained quantum transistors produce the 3-qubit outputs, this way developing graphentronic integrated circuits for the use in quantum computing framework.

Adopting the laws of Boolean Algebra, quantum tunneling activation of GO/ZnO depositions is a favorable approach for measuring the logical outcome of the gates. With the aid of quantum Hamiltonian computing (QHC) gate working principle, it is possible to express the quantum level repulsion effect that takes place when stretching the graphenic valence-conduction band gap, as well as the description of quantum interferences that result in synergic tunneling transport [33].

ACKNOWLEDGEMENT

Authors acknowledge the contribution to this work within the Nucleus-Programme under the project PN-19-22-01-02 and of its 2020 renewal as funded by the Romanian Ministry of Education and Research.

REFERENCES

1. Pastrana-Martínez, L.M.; Morales-Torres, S.; Figueiredo, J.L.; Faria, J.L.; Silva, A.M.T. Graphene photocatalysts. In Multifunctional Photocatalytic Materials for Energy; Woodhead Publishing in Materials volume series, 1st Edition; Lin, Z.; Ye, M.; Wang, M.; Elsevier Science, 2018; pp. 79-101.
2. Novoselov, K.S.; Geim, A.K.; Morozov, S.V.; Jiang, D.; Zhang, Y.; Dubonov, S.V.; Grigorieva, I.V.; Firsov, A.A. Electric field effect in atomically thin carbon films. Science 2004, 306:5696, 666-669.
3. Geim, A.K. Graphene: status and prospects. Science 2009, 324:5934, 1530-1534.

4. Wang, J.; Ma, F.; Liang, W.; Sun, M. Electrical properties and applications of graphene, hexagonal boron nitride (h-BN), and graphene/h-BN heterostructures. Materials Today Physics 2017, 2, 6-34.
5. Avouris, P. Graphene: electronic and photonic properties and devices. Nano Letters 2010, 10:11, 4285-4294.
6. Castro Neto, A.H.; Guinea, F.; Peres, N.M.R.; Novoselov, K.S.; Geim, A.K. Reviews of Modern Physics. 2009, 81, 109–162.
7. Dissanayake, D.M.N.M.; Eisaman, M.D. Chemical-free n-type and p-type multilayer-graphene transistors. Applied Physics Letters 2016, 109, 0531101-0531103.
8. Phan, D.T.; Chung, G.S. P–n junction characteristics of graphene oxide and reduced graphene oxide on n-type Si (111). Journal of Physics and Chemistry of Solids 2013, 74:l1, 1509-1514.
9. Mathkar, A.; Tozier, D.; Cox, P.; Ong, P.; Galande, C.; Balakrishnan, K.; Reddy, A.L.M.; Ajayan, P.M. Controlled, stepwise reduction and band gap manipulation of graphene oxide. Journal of Physical Chemistry Letters 2012, 3:8, 986-991.
10. Phillips, P. Motness. Annals of Physics 2006, 321:7, 1634-1650.
11. Lindvall, N. Towards graphene-based devices: Fabrication and characterization, Ph.D. dissertation, Chalmers University of Technology, 2012.
12. Resch, S.; Karpuzcu, U.R. Quantum Computing: An Overview Across the System Stack 2019, 1-29.
13. Griffiths, R.B. Consistent quantum theory. Cambridge University Press, 2003.
14. Nielsen, M.A.; Chuang, I.L. Quantum computation and quantum information, 2000.
15. Wolf, de R. Quantum Computing:Lecture Notes, 2019.
16. Jaeger, G. What in the (quantum) world is macroscopic? American Journal of Physics 2014, 82:9, 896–905.
17. Aspuru-Guzik, A.; Dutoi, A.D.; Love, P.J.; Head-Gordon, M. Simulated quantum computation of molecular energies. Science. 2005, 309:5741, 1704–1707.
18. Wecker, D.; Hastings, M.B; Troyer, M. Progress towards practical quantum variational algorithms. Physical Review A 2015, 92: 4, 042303.
19. Leuenberger M.N, Loss, D. Quantum computing in molecular magnets. Nature 2001, 410:6830, 789.
20. Cory, D.G.; Fahmy, A.F.: Havel, T.F. Ensemble quantum computing by nmr spectroscopy. Proceedings of the National Academy of Sciences 1997, 94:5, 1634–1639.
21. Milburn, G.J. Photons as qubits. Physica Scripta, 2009, T137, 014003.
22. Kitaev, A.Y. Fault-tolerant quantum computation by anyons. Annals of Physics 2003, 303:1, 2–30.
23. Cirac J.I.; Zoller, P. Quantum computations with cold trapped ions. Physical review letters 1995, 74:20, 4091.
24. Veldhorst, M.; Yang, C.H.; Hwang, J.C.C.; Huang, W.; Dehollain, J.P.; Muhonen, T.; Simmons, S.; Laucht, A.; Hudson, F.E.; Itoh, K.M. A two-qubit logic gate in silicon. Nature 2015, 526:7573, 410.
25. Brecht, T.; Pfaff, W.; Wang, C.; Chu, Y.; Frunzio, L.; Devoret, M.H.; Schoelkopf, R.J. Multilayer microwave integrated quantum circuits for scalable quantum computing. npj Quantum Information 2016, 2, 16002.

26. DiCarlo, L.; Chow, J.M.; Gambetta, J.M.; Bishop, L.S.; Johnson, B.R.; Schuster, D.I.; Majer, J.; Blais, A.; Frunzio, L.; Girvin, S.M. Demonstration of two-qubit algorithms with a superconducting quantum processor. Nature 2009, 460:7252, 240.
27. Cataldo, F.; Putz, M.V.; Ursini, O.; Angelini, G.; Garcia-Hernandez, D.A.; Manchado, A. A new route to graphene starting from heavily ozonized fullerenes: Part 3 – an electron spin resonance study, Fullerenes, Nanotubes and Carbon Nanostructures 2016, 24:3, 195-201.
28. Tomadin, A.; Hornett, S.M.; Wang, H.I.; Alexeev, E.M.; Candini, A.; Coletti, C.; Turchinovich, D.; Kläui, M.; Bonn, M.; Koppens, F.H.L.; Hendry, E.; Polini, M.; Tielrooij, K.J. The ultrafast dynamics and conductivity ofphotoexcited graphene at different Fermi energies, Science Advances 2018, 4:5, 5313:1-10.
29. Srivastava, S.; Kino, H.; Joachim, C. Quantum half-adder Boolean logic gate with anano-graphene molecule and graphene nano-electrodes, Chemical Physics Letters, Elsevier 2017, 667, 301-306.
30. Wang, J.I.; Rodan-Legrain, D.; Bretheau, L.; Campbell, D.L.; Kannan, B.; Kim, D.; Kjaergaard, M.; Krantz, P.; Samach, G.O.; Yan, F.; Yoder, J.L.; Watanabe, K.; Taniguchi, T.; Orlando, T.P.; Gustavsson, S.; Jarillo-Herrero, P.; Oliver, W.D. Coherent control of a hybrid superconducting circuit made with graphene-based van der Waals heterostructures, Nature Nanotech. 2019, 14, 120–125.
31. Krantz, P.; Kjaergaard, M.; Yan, F.; Orlando, T.P.; Gustavsson, S.; Oliver, W.D. A quantum engineer's guide to superconducting qubits, Appl. Phys. Rev. 2019, 6:0213181, 1-57.
32. Namarvar, O.F.; Giraud, O.; Georgeot, B.; Joachim, C. Quantum Hamiltonian Computing protocols for molecular electronics Boolean logic gates, Quantum Sci. Technol. 2019, 4:035009, 1-24.
33. Tahan, C. Graphene qubit motivates materials science. Nature Nanotech. 2019, 14(2), 102–103.